Check for updates

The FEBS Journal

FEBS PRESS science publishing by scientists

Structures of lactaldehyde reductase, FucO, link enzyme activity to hydrogen bond networks and conformational dynamics

Alberto Zavarise[1], Shruthi Sridhar[1,2], Tiila-Riikka Kiema[2], Rikkert K. Wierenga[2] and Mikael Widersten[1]

1 Department of Chemistry – BMC, Uppsala University, Sweden
2 Faculty of Biochemistry and Molecular Medicine, University of Oulu, Finland

Keywords
catalytic mechanism; crystal structures; lactaldehyde reductase; stereoselectivity

Correspondence
R. K. Wierenga, Department of Chemistry – BMC, Uppsala University, Box 576, SE-751 23 Uppsala, Sweden
Tel: +358 407 486 439
E-mail: rik.wierenga@oulo.fi
and
M. Widersten, Faculty of Biochemistry and Molecular Medicine, University of Oulu, FIN-90014 Oulu, Finland
Tel: +46 18 471 4992
E-mail: mikael.widersten@kemi.uu.se

Alberto Zavarise and Shruthi Sridhar contributed equally to this article

(Received 10 March 2022, revised 17 July 2022, accepted 22 August 2022)

doi:10.1111/febs.16603

A group-III iron containing 1,2-propanediol oxidoreductase, FucO, (also known as lactaldehyde reductase) from *Escherichia coli* was examined regarding its structure–dynamics–function relationships in the catalysis of the NADH-dependent reduction of (2*S*)-lactaldehyde. Crystal structures of FucO variants in the presence or absence of cofactors have been determined, illustrating large domain movements between the apo and holo enzyme structures. Different structures of FucO variants co-crystallized with NAD^+ or NADH together with substrate further suggest dynamic properties of the nicotinamide moiety of the coenzyme that are important for the reaction mechanism. Modelling of the native substrate (2*S*)-lactaldehyde into the active site can explain the stereoselectivity exhibited by the enzyme, with a critical hydrogen bond interaction between the (2*S*)-hydroxyl and the side-chain of N151, as well as the previously experimentally demonstrated pro-(*R*) selectivity in hydride transfer from NADH to the aldehydic carbon. Furthermore, the deuterium kinetic isotope effect of hydride transfer suggests that reduction chemistry is the main rate-limiting step for turnover which is not the case in FucO catalysed alcohol oxidation. We further propose that a water molecule in the active site – hydrogen bonded to a conserved histidine (H267) and the 2′-hydroxyl of the coenzyme ribose – functions as a catalytic proton donor in the protonation of the product alcohol. A hydrogen bond network of water molecules and the side-chains of amino acid residues D360 and H267 links bulk solvent to this proposed catalytic water molecule.

Introduction

Alcohol dehydrogenases (ADHs, EC1.1.1.1) are among the most-studied enzyme super families and have stood as exemplifying models for such central mechanistic principles of catalysis as hydrogen tunnelling [1–4], low-barrier hydrogen bonds [5], transition metal afforded electrophilic catalysis [6] and NAD(P)-dependent hydride transfer [7,8]. Alcohol dehydrogenases have also been the paradigm of sequential BiBi reactions with their variations [9–16]. Most of this knowledge has been gathered on systems belonging to the zinc (II)-dependent group I family of enzymes [17,18].

The less studied group III ADHs, so far identified only in microbes [20], depend on Fe(II) as cofactor. We have been interested in a group III ADH involved

Abbreviations
ADH, alcohol dehydrogenase; ADPR, adenosine diphosphate ribose; EDO, ethylene glycol; KIE, kinetic isotope effect; NAD^+, nicotinamide dinucleotide oxidized form; NADD, [4*R*-^{2}H]-NADH, NADH, nicotinamide dinucleotide reduced form; PDB, Protein Data Bank.

This is an open access article under the terms of the Creative Commons Attribution-NonCommercial License, which permits use, distribution and reproduction in any medium, provided the original work is properly cited and is not used for commercial purposes.

17424658, 2023, 2, Downloaded from https://febs.onlinelibrary.wiley.com/doi/10.1111/febs.16603 by Uppsala University Karin Boye, Wiley Online Library on [17/03/2023]. See the Terms and Conditions (https://onlinelibrary.wiley.com/terms-and-conditions) on Wiley Online Library for rules of use; OA articles are governed by the applicable Creative Commons License

in the secondary metabolism of rare sugars in *Escherichia coli*, FucO (EC1.1.1.77, Fig. 1) [21–23], with the ambition to employ its regiospecificity for primary alcohol oxidation in the biocatalysis of vicinal diols to α-hydroxy aldehydes [24,25]. The proposed physiological substrate of this enzyme is (2*S*)-lactaldehyde (compound **2** in Fig. 2), with the resulting (2*S*)-1,2-propanediol (**4**) as the ultimate fermentation product in the metabolism of L-fucose [21,22]. A primary role as aldehyde reductase is suggested from the pH dependencies of catalysis where aldehyde reduction is insensitive to pH within a broad range, whereas alcohol oxidation increases linearly with pH up to at least pH 10, with the enzyme being virtually inactive at neutral pH values [23]. The substrate scope of FucO is limited to short-chain aldehydes and α-hydroxyaldehydes and their cognate alcohols and vicinal diols with a strong preference for the (*S*)-enantiomer of the substrates [23]. The catalytic mechanism of FucO has been inferred from knowledge gained from studies of group I alcohol dehydrogenases such as the horse liver [17] or yeast [18] ADH. However, considering the substantial differences in structure and metal cofactor dependencies between these ADHs, it is questionable as to how much of the understanding based on the structure–function–dynamics properties of group I ADHs can be applied to group III isoenzymes. Thus, here we have continued studies on the catalytic mechanism of FucO, focusing on the presumed native aldehyde reductase function.

FucO is a dimeric enzyme and each subunit consists of two domains, being a nucleotide-binding domain, which binds the cofactor (NAD^+ or NADH, consisting of residues 1 to 180) and a C-terminal domain which binds the Fe(II) active-site metal ion (residues 190–380). Both domains contribute to the dimer interface and both domains contribute to the binding groove to which the cofactor NAD^+/NADH and substrate bind in the ternary complex. Here, we show that the domains can adopt "open" (in the absence of nucleotide) and "closed" conformations (in the presence of nucleotide). The new structural and enzymological data also provide insight into the FucO reaction mechanism.

Results and Discussion

Enzyme kinetics

We have focused here on the reductive direction of the catalysed reaction, based on the presumption that (*S*)-lactaldehyde **2** is the enzyme's physiological substrate. Apparent steady-state parameters determined with **2**, propanal (**1**) and the coenzyme NADH are given in Table 1. The obtained substrate saturation curves exhibited significant ($P < 0.01$) positive cooperativity and could not be adequately modelled by the Michaelis–Menten expression. Instead, a modified Hill equation (Eq. 1) was employed for modelling the kinetic behaviour. Thus, the parameter describing half-

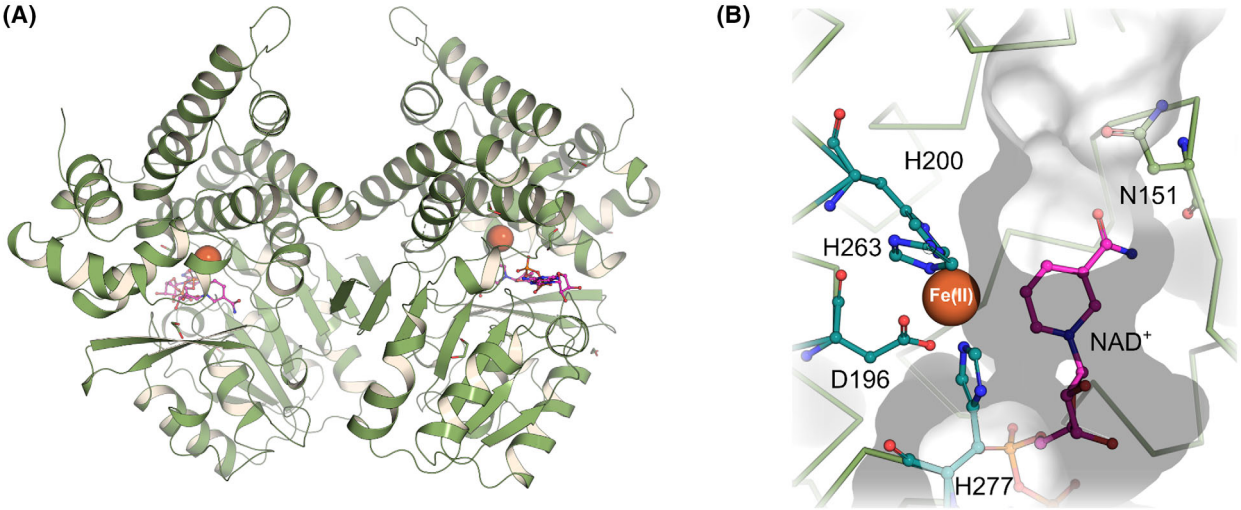

Fig. 1. (A) Cartoon representation of the homodimeric structure of FucO (F254I, PDB entry 7QNJ). The two catalytic Fe(II) ions are shown as rust coloured spheres and the NAD^+ coenzymes in magenta coloured ball-and-stick representation. (B) Close-up of the active site (A-chain). Active-site residues discussed in this work are shown in ball-and-stick representation. Image constructed in PYMOL ver. 2.5 [19].

17424658, 2023, 2, Downloaded from https://febs.onlinelibrary.wiley.com/doi/10.1111/febs.16603 by Uppsala University Karin Boye, Wiley Online Library on [17/03/2023]. See the Terms and Conditions (https://onlinelibrary.wiley.com/terms-and-conditions) on Wiley Online Library for rules of use; OA articles are governed by the applicable Creative Commons License

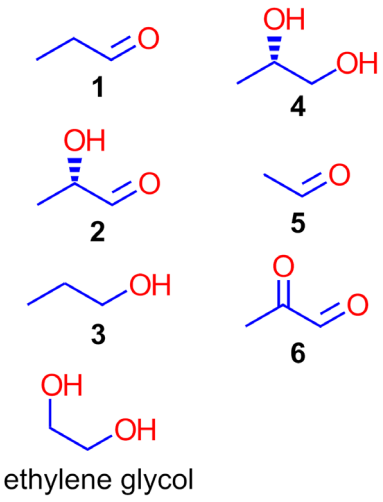

Fig. 2. Compounds discussed.

saturation of substrate, K_M, has been replaced by "$K_{0.5}$" to emphasize that this parameter is not directly equivalent to a Michaelis constant. The exponent n_H is the Hill coefficient.

$$\frac{v_0}{[E]_{tot}} = \frac{k_{cat}[S]^{n_H}}{K_{0.5}^{n_H} + [S]^{n_H}} \quad (1)$$

The lower determined turnover number in the reactions with constant concentration of **2** and varied NADH, as compared to the reciprocal combination, is not easily explained. In both cases were saturating concentrations of the non-varied substrates present in the respective reaction mixtures, yet the k_{cat} values differ by a factor of 3. If the observed behaviour may be linked to the cooperative behaviour and the complexity of the kinetic mechanism (*vide infra*) is unclear.

FucO has been proposed to follow an ordered BiBi mechanism in the oxidation of alcohols based on a relatively small primary deuterium kinetic isotope effect (KIE) on k_{cat} (1.9) in the oxidation of 1-propanol (**3**) and a high dependency of medium viscosity on k_{cat} in the oxidation of **4** [23]. The rate-limiting steps of catalysis have not been firmly pinpointed, however. The kinetic mechanism of the reductive reaction has not previously been established. Thus, we analysed the product inhibition pattern of the reductive reaction involving NADH and **2**. The double reciprocal plots of the four possible combinations are shown in Fig. 3, with the numerical values of determined steady-state parameters in Table S1. The interpretation of the resulting inhibition pattern is complicated by the fact that all substrate/product combinations exhibited different degrees of cooperativity. We have therefore based the assignment of inhibition type on the influence of the inhibitors on the estimated apparent V_{max} and $K_{0.5}$ values (Table S1). The interpreted inhibition patterns are given in Fig. 3E and resemble mostly that of a rapid equilibrium ordered BiBi with a dead-end enzyme-EAP complex [26], although the assignment should be regarded as preliminary considering the non-typical behaviour. Furthermore, the presence of the inhibiting products also alters the cooperative behaviour, in some cases, quite dramatically. For instance, in the reactions with constant [**2**] (substrate "B") and varied [NADH] (substrate "A"), addition of NAD^+ (product "Q") alters the positive cooperativity (n_H = 1.3–1.6) to negative cooperativity

Table 1. Apparent steady-state kinetic parameters of aldehyde reduction.

Enzyme	Substrate	k_{cat} (s^{-1})	$K_{0.5}$ (mM)	$k_{cat}/K_{0.5}$ ($s^{-1}\cdot mM^{-1}$)	n_H (Hill coeff.)	k_1 ($s^{-1}\cdot mM^{-1}$)	k_{-1} (s^{-1})	K_1[a] (mM)
Wild type	NADH	3.5 ± 0.3[b]	0.038 ± 0.004[b]	91 ± 10[b]	1.6 ± 0.1	2100 ± 300	74 ± 10	0.035 ± 0.007
H267Q	NADH	3.6 ± 0.4[c]	0.21 ± 0.04[c]	17 ± 4[c]	1.4 ± 0.2	1100 ± 200	36 ± 10	0.032 ± 0.01
D360N	NADH	≥9.5[c]	≥0.26[c]	36[c]	0.71 ± 0.1	2000 ± 300	29 ± 10	0.015 ± 0.007
Wild type	**1**	24 ± 2	1.9 ± 0.4	12 ± 3	1.4 ± 0.4			
H267Q	**1**	15 ± 0.6	15 ± 1	0.95 ± 0.09	1.7 ± 0.2			
D360N	**1**	11 ± 0.9	22 ± 5	0.51 ± 0.09	(1)			
Wild type	**2**	11 ± 0.3	0.31 ± 0.02	36 ± 3	1.5 ± 0.2			
Wild type	**2** + NADD[d]	5.1 ± 0.2	0.25 ± 0.02	20 ± 2	1.2 ± 0.2			
H267Q	**2**	9.8 ± 0.7	9.9 ± 1	1.0 ± 0.09	(1)			
H267Q	**2** + NADD[d]	7.3 ± 0.9	18 ± 4	0.42 ± 0.05	(1)			
D360N	**2**	14 ± 0.6	2.5 ± 0.4	5.5 ± 0.6	(1)			
Wild type	**5**	7.3 ± 0.2[e]	11 ± 1[e]	0.65 ± 0.04[e]	-			
Wild type	**6**	10 ± 0.2[e]	4.1 ± 0.3[e]	2.5 ± 0.1[e]	-			

[a]$K_1 = k_{-1}/k_1$.; [b]Determined in the presence of 4 mM **2**.; [c]Determined in the presence of 30 mM **1**.; [d]In the presence of [4*R*-^{2}H]-NADH : NADH (50 : 50).; [e]Data from ref. [23].

17424658, 2023, 2, Downloaded from https://febs.onlinelibrary.wiley.com/doi/10.1111/febs.16603 by Uppsala University Karin Boye, Wiley Online Library on [17/03/2023]. See the Terms and Conditions (https://onlinelibrary.wiley.com/terms-and-conditions) on Wiley Online Library for rules of use; OA articles are governed by the applicable Creative Commons License

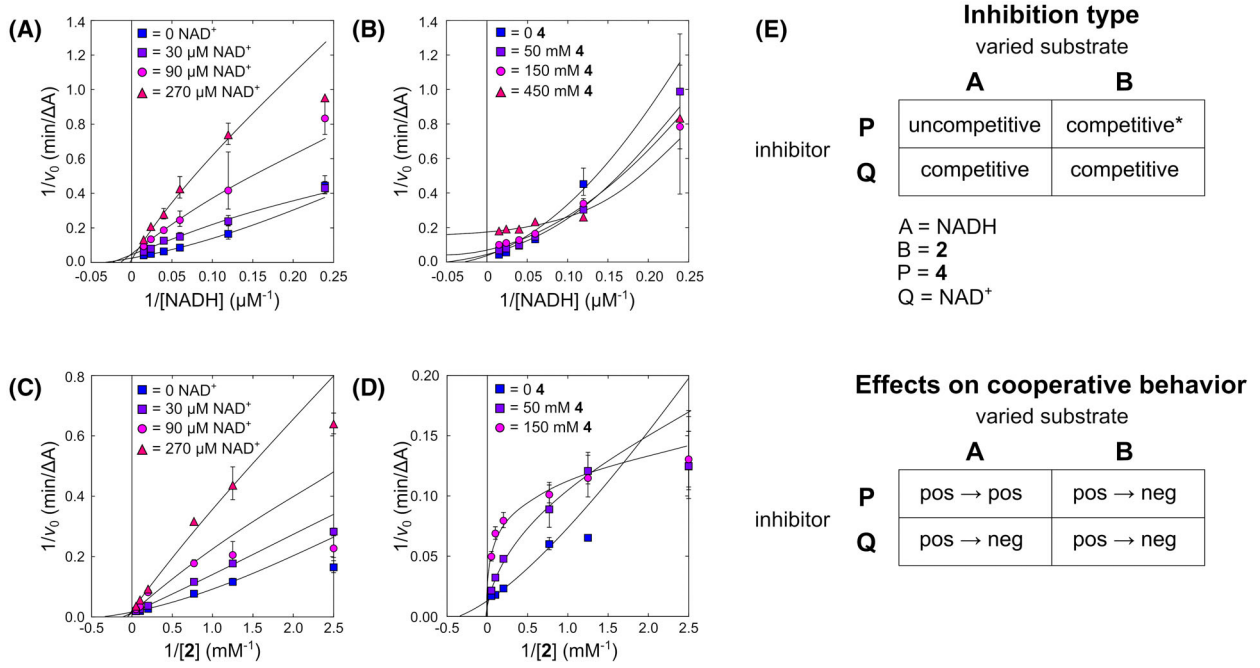

Fig. 3. Product inhibition of the catalysed reduction of **2**. (A–D) Plots of $1/v_0$ versus 1/[varied S]. The non-varied substrate was present at > 10 × $K_{0.5}$. (E) Interpretation of the inhibition patterns based on the effects on the apparent V_{max} and $K_{0.5}$ parameters. The starred B/P pair (panel D) exhibits a dramatic shift in cooperative behaviour from positive in the absence of P to pronounced negative cooperativity with increasing concentrations of alcohol **4**. Error bars are standard deviations of initial velocities ($n = 4$). The asterisk only emphasizes the extreme response observed in that product ("P")/substrate ("B") pair.

(n_H = 0.82–0.73). A summary of the effects on cooperativity is also provided in Fig. 3E.

The underlying mechanism for the shift in cooperative behaviour is unclear. It is possible that the inhibitor competes for binding at one subunit forming a dead-end enzyme-EQB or EAP complex. Such futile ternary complexes may cause conformational changes that are communicated to the neighbouring subunit, causing a lowering of the affinity for NADH at the catalytically competent subunit. We describe later in the current work crystal structures of the enzyme in open and closed states, with quite different intersubunit contacts that are in agreement with possible communication of structural changes between the respective active sites of the dimer.

Allosteric behaviour in metabolic enzymes is common, since it allows for emphasized responses to both substrate and product concentrations in the context of reaction networks maintaining homeostasis [27,28]. A physiological scenario where NADH is present at enzyme-saturating concentrations and the concentrations of aldehyde **2** are varied, depending on the presence of sugar metabolites, is possible. Thus, the observed substantial shift from positive to negative cooperativity in the reaction with varied [**2**], saturating [NADH], and added alcohol **4**, may reflect a sensor for intracellular accumulation of the diol, which is of no apparent metabolic value. Diol **4** may even interact with related enzyme systems in unfavourable side-reactions.

The primary deuterium KIE in the reaction with [4*R*-^{2}H]NADH and **2** resulted in a value higher than that for 1-propanol oxidation, 4.4 (±0.2) as compared to 1.9 (±0.1) (Table 2). Adopting the model of Northrop including commitment-to-catalysis arguments [29], a smaller deuterium KIE on k_{cat} suggests that reaction steps downstream of the isotope sensitive step, i.e. the hydride transfer, are rate limiting for turnover, for instance product release steps. Here, the $^{D}k_{cat}$ of 4.4 rather suggests that chemistry of reduction is rate limiting to a higher degree as compared to the alcohol oxidation. The $^{D}k_{cat}/K_{0.5}$ was similar (3.5 ± 0.5) to that previously determined for propanol oxidation (4.2 ± 0.4).

It has been shown in related systems with group I ADHs [15,16] that turnover numbers are often comparable to steps involved in coenzyme release, i.e. NAD^+ release (k_5) in the present case. Due to the lack of a spectral probe for association and dissociation of the oxidized coenzyme, we were unable to determine the

17424658, 2023, 2, Downloaded from https://febs.onlinelibrary.wiley.com/doi/10.1111/febs.16603 by Uppsala University Karin Boye, Wiley Online Library on [17/03/2023]. See the Terms and Conditions (https://onlinelibrary.wiley.com/terms-and-conditions) on Wiley Online Library for rules of use; OA articles are governed by the applicable Creative Commons License

Table 2. Kinetic isotope effects.

Enzyme	Reduction of **2**[a]		Reduction of **1**[b]	Oxidation of **3**[c]	
	$^{D}k_{cat}$	$^{D}k_{cat}/K_{0.5}$	$^{H2O}k/^{D2O}k$	$^{D}k_{cat}$	$^{D}k_{cat}/K_{M}$
wild-type	4.4 ± 0.2	3.5 ± 0.5	0.99 ± 0.1	1.9 ± 0.07	4.2 ± 0.4
H267Q	2.7 ± 0.4	4.9 ± 0.7	0.38 ± 0.08	–	–
D360N	–	–	0.50 ± 0.1	–	–

[a]Kinetic isotope effect (KIE) of hydride transfer from [4*R*-^{2}H]-NADH to **2**.; [b]Solvent deuterium KIE of reduction of **1**, at pL = 8.0, expressed as the ratio of k_{cat}^{app} in H_2O as compared to D_2O.; [c]KIE of hydride transfer from 1,1-d_2-propanol to NAD^+ at pH 10.0 [23].

NAD^+ off-rate for an evaluation of the rate limitation of this step in the catalytic cycle. We can, however, conclude that the dissociation rate of NADH (k_{-1} in Table 1) exceeds k_{cat} for **2** by 6.7-fold and if NAD^+ affinity is similar to that of NADH, which is suggested from their respective $K_{0.5}$ values (38 and 70 μM for NADH and NAD^+, respectively [23]), it would infer that cofactor release is not rate limiting to any major extent in the catalysed aldehyde reduction. This is in line with the fact that k_{cat} of the reduction of **1** is only partially affected by increase in medium viscosity [23] which plays down the influence of product release being rate limiting for turnover. The substantial primary deuterium KIE in the reduction of **2** is in agreement with that presumption.

Substrate selectivity

(2*S*)-Lactaldehyde (**2**) is the proposed physiological substrate and the value of $k_{cat}/K_{0.5}$ exceeds all other aldehyde substrates tested to this point with the wild-type enzyme by > 3-fold (Table 1). The higher enzyme efficiency is mainly caused by a relatively low $K_{0.5}$ for **2**, which is fivefold lower compared to that of propanal and 11-fold lower compared to that of 2-oxopropanal (**6**). This implies that stereoselective interactions involving the (2*S*)-hydroxyl of **2** are at play in productive substrate binding, which is further supported by the strong, 300-fold, preference for (2*S*)-propane-1,2-diol over the (2*R*) enantiomer in the oxidative reaction direction [23].

Lack of available crystal structures where informative ligands are bound in putatively productive modes in the active site has hampered a conclusive description of the observed stereoselectivity in FucO. Examination of the structure of wild-type FucO (PDB entry 1RRM [30]), in the light of functional data on isolated active-site mutants that have lost the enantioselectivity [25], points out residue N151 as a plausible determinant of the (2*S*)-selectivity. Its involvement may be attributed to a direct interaction between the C-2 hydroxyl of the substrate with the amide side-chain of N151, as suggested from manually docking this substrate into a putatively productive binding mode within the active site (Fig. 4).

Catalytic mechanism

The established mechanism for group I ADHs has been a starting point when analysing the catalytic mechanism of FucO. The iron(II) cofactor is assumed to act as an electrophile stabilizing the buildup of negative charge on the carbonyl oxygen upon hydride transfer from NADH to the aldehyde C-1 (Fig. 5A). The Fe(II) ion is coordinated by the side-chains of three histidines, one aspartate and in addition, in the unliganded active site, by two waters. It concerns the NE2-atoms of His200, His263 and His277 and the OD1-atom of Asp196 (Fig. 5B–D). These residues protrude out of three different helices of the helical domain. The two water molecules are displaced in the presence of the bound nicotinamide ring in complexes with NAD^+ and NADH, as also observed in the structural studies of a bacterial FucO homologue [31] for which structures are available of the unliganded enzyme (complexed with Fe(II)) and of the binary complex (with bound Fe(II) and NAD^+ in the active site) The coordination of the Fe(II) ion is also observed in the structure of 1,3-propanediol dehydrogenase (PDB entry 3BFJ [32]), also in this case the structure is available for the enzyme complexed with Fe(II), but in the absence of NAD^+. Homologues also from other sources display very similar Fe(II) coordination and amino acid ligands [33–35].

The pro-(*R*) hydride of NADH is transferred to the substrate carbonyl in the reduction reaction [23]. In this work, we have solved structures of FucO variants in complex with NADH (PDB entry 7R5T) and NAD^+ (PDB entries 7QNF, 7QNJ and 7R0P). These FucO variants have been identified previously in directed evolution studies aimed at finding variants with different substrate specificities and we have confirmed that these variants still catalyse the FucO reaction with the natural substrate (Shruthi Sridhar, manuscript in preparation). The crystal structures of the complexes of these variants with NADH and NAD^+ show that

17424658, 2023, 2, Downloaded from https://febs.onlinelibrary.wiley.com/doi/10.1111/febs.16603 by Uppsala University Karin Boye, Wiley Online Library on [17/03/2023]. See the Terms and Conditions (https://onlinelibrary.wiley.com/terms-and-conditions) on Wiley Online Library for rules of use; OA articles are governed by the applicable Creative Commons License

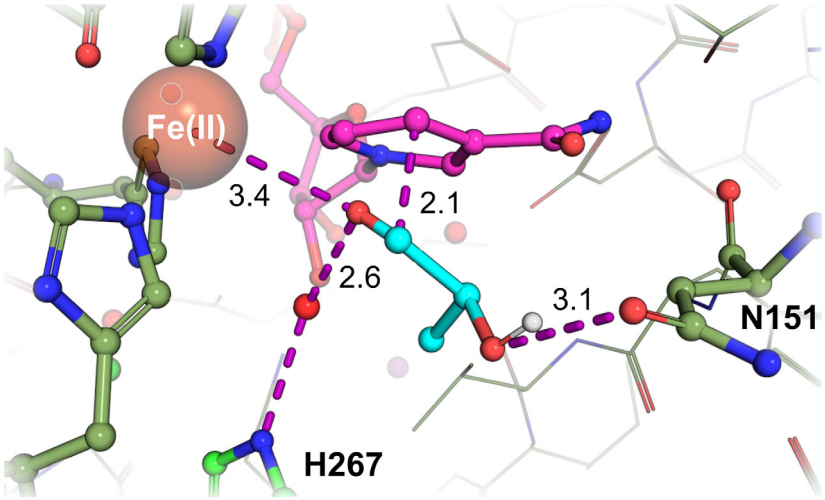

Fig. 4. Modelling of **2** (cyan coloured carbons) in the active site of FucO as described in Materials and methods. The NADH molecule is coloured magenta. A hydrogen bond between the side-chain amide of N151 and the (2*S*)-hydroxyl of **2** is clearly possible in the modelled conformation. The carbonyl oxygen is within interacting distance of the iron(II) and the carbonyl carbon is located at a distance (2.1 Å) and angle from C-4 of the nicotinamide of the coenzyme that could allow for transfer of the pro-(*R*) hydride to the carbonyl carbon, consistent with previous experimental evidence for pro-(*R*) selectivity in FucO [23]. The modelled conformation agrees with the mode of binding of ethylene glycol (EDO) (a *bona fide* substrate [23]) observed in the crystal structure of FucO (N151G/L259V) (Fig. 6B).

the mode of binding of the nicotinamide ring is in agreement with the experimental evidence for the stereoselectivity in hydrogen transfer from NADH (Fig. 4). The crystal structures of the point mutated variants F254I, L259V and (N151G/L259V) determined at high resolution (Table 3), respectively, at 1.73 Å (7QNI), 1.66 Å (7QNJ) 1.6 Å (7R0P), 1.85 Å (7R5T), 1.4 Å (7R3D) and 2.14 Å (7QNF), show that the point mutations cause only local changes in the structure; also, the relative positions of the two domains in the holo structures are the same as in wild type (Shruthi Sridhar, manuscript in preparation). In all crystal structures that we have determined, whenever an alcohol or aldehyde analogue is bound in what can be regarded as mimicking productive enzyme–substrate complexes, the nicotinamide ring of the coenzyme is invisible in the electron density maps (Fig. 6). As an example, in the crystal structure of FucO (N151G/L259V, PDB entry 7QNF) complexed with ADP-ribose (ADPR) and ethylene glycol, one of the hydroxyl oxygens of this alcohol is located at the same position bound to the Fe(II) as a water molecule otherwise present (Fig. 6B). In structures where there is no ligand bound, or the nicotinamide ring is absent, two water molecules bound to the Fe(II) are present (Fig. 6A). If the nicotinamide moiety is included back in the coenzyme, steric clashes with both water molecules occur. We have interpreted these observations as capturing different states of the coenzyme bound in the active site. In the binary E•NADH or E•NAD^+ complex, the nicotinamide ring of the coenzyme is positioned in a conformation close to the Fe(II) cofactor that may prevent productive binding of the aldehyde substrate. Thus, the structural data clearly suggest that dynamic movement of the nicotinamide ring is necessary for the formation of a competent ternary complex (which could not be captured in a crystal structure), thereby allowing catalysis to occur. Formation of the product alcohol involves protonation of the intermediate alkoxide. A potential proton donor is a water molecule (circled in Fig. 7) that is within close hydrogen bond distance to the carbonyl oxygen of **2** modelled in an assumed productive binding mode, thus perfectly positioned for protonation of the formed oxide. Possible links between structural dynamics in the active site and the cooperative behaviour in the kinetics are still unclear.

Two active-site residues that appear to be conserved within this protein family (Fig. S1), H267 and D360 (FucO numbering), are within hydrogen bond distance to each other, forming an interaction network together with the main-chain amides of V361 and C362 (Fig. 7). H267 is also hydrogen bonded to the above-mentioned candidate catalytic water molecule. Furthermore, a chain of hydrogen bonds of additional water molecules together with the carboxyl groups of D360 links the substrate bonded water molecule to bulk solvent (Fig. 7), ensuring an equilibrated supply of

17424658, 2023, 2, Downloaded from https://febs.onlinelibrary.wiley.com/doi/10.1111/febs.16603 by Uppsala University Karin Boye, Wiley Online Library on [17/03/2023]. See the Terms and Conditions (https://onlinelibrary.wiley.com/terms-and-conditions) on Wiley Online Library for rules of use; OA articles are governed by the applicable Creative Commons License

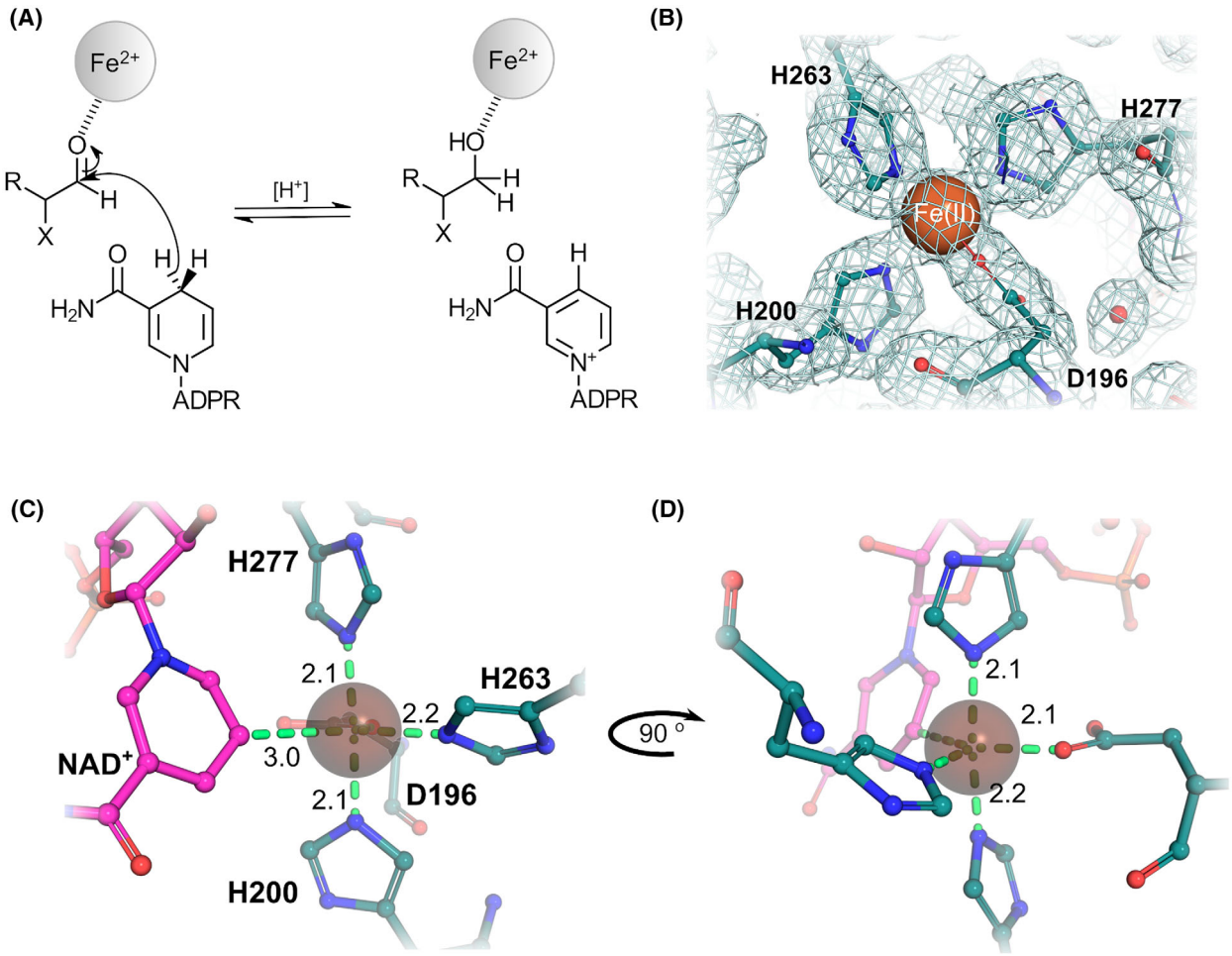

Fig. 5. (A) Model of the basic mechanism of FucO catalysed aldehyde reduction, with the iron(II) cofactor acting as electrophile stabilizing a transient oxyanion. The pro-(*R*) hydride of NADH is transferred to the substrate. (B–D) Coordination of Fe(II) cofactor in FucO. (B) $2F_oF_c$ map drawn at 1σ of the residues liganding to the Fe(II) centre (A-chain of PDB entry 7QNJ). (C, D) Distances (in Å) between Fe(II) and ligands. The three histidine ligands and D196 bind the central ion at close to 90° angles. The C-5 carbon of bound NAD^+ is also within Van der Waals distance to the iron(II). Image constructed in PYMOL ver. 2.5.

protons for catalysis. The acid/base properties of the imidazolium/imidazole of H267, and with its acid/base characteristics influenced by the presence of D360, made us substitute both these residues to their closest isosteres (H267Q and D360N) for analysis of possible contributions to catalysis.

The absence of a solvent deuterium KIE on the apparent k_{cat} values determined with propanal (**1**) of the wild-type catalysed reduction suggests that proton transfer events are not contributing to rate limitations (Table 2, Fig. 8). The H267Q or D360N substitutions do not affect the turnover numbers with either **1** or **2** (Table 1), therefore rate-limiting acid/base roles for these residues can be excluded. The approximately 2-fold lower k_{cat} values in Table 1 should be viewed as lower limit values, since the increased $K_{0.5}$ NADH displayed by both mutants prevents full enzyme saturation in the assays.

Although turnover numbers are in essence unaffected by the H267Q and D360N substitutions, the effects on $K_{0.5}$ values are quite pronounced. The half-saturation values for either aldehyde, **1** or **2**, are increased 8- to 32-fold (Table 1). If assuming a (mainly) ordered sequential kinetic mechanism, K_M for the aldehyde substrate, "K_{MB}" can be described by Eqn (2) [13], where the rate constant designations refer to the ordered mechanism shown in Scheme 1. A reasonable assumption is that aldehyde association rates are considerably faster than subsequent steps of reduction and alcohol release. Eqn (2) can then

17424658, 2023, 2, Downloaded from https://febs.onlinelibrary.wiley.com/doi/10.1111/febs.16603 by Uppsala University Karin Boye, Wiley Online Library on [17/03/2023]. See the Terms and Conditions (https://onlinelibrary.wiley.com/terms-and-conditions) on Wiley Online Library for rules of use; OA articles are governed by the applicable Creative Commons License

Table 3. Data collection, data processing and refinement statistics.

FucO variants	L259V (apo)	F254I co-crystallized with NAD^+ and Fe(II)	F254I co-crystallized with NAD^+ and Fe(II)	F254I co-crystallized with NADH and Fe(II)	N151G/L259V co-crystallized with NADH and Fe(II)	N151G/L259V co-crystallized with NAD^+ and Fe(II)
Cryoprotectant	Glycerol	Glycerol	Ethylene glycol	Glycerol	Glycerol	Ethylene glycol
Data collection						
Beamline	PETRA III (P14)	DLS (I03)	DLS (I03)	DLS (I24)	DLS (I24)	DLS (i03)
Detector	EIGER2 CdTe 16 M	Eiger2 XE 16 M	Eiger2 XE 16 M	Pilatus3 6 M	Pilatus3 6 M	Eiger2 XE 16 M
Wavelength (Å)	0.9762	0.9763	0.9763	0.9999	0.9999	0.97625
Temperature (K)	100	100	100	100	100	100
Data processing						
Space group	C2 2 2_1	$P2_12_12_1$	$P2_12_12_1$	$P2_1$	$P2_1$	$P2_12_12_1$
a, *b*, *c* (Å)	55.41, 108.36, 123.90	58.14, 86.22, 148.47	57.98, 86.16, 147.65	69.56, 54.33, 101.80	62.96, 95.11, 69.36	61.83, 85.76, 136.68
α, β, γ (°)	90.00, 90.00, 90.00	90.00, 90.00, 90.00	90.00, 90.00, 90.00	90.00, 99.97, 90.00	90.00, 116.48, 90.00	90.00, 90.00, 90.00
Data processing software	XDS, AIMLESS	XDS, AIMLESS	DIALS, AIMLESS	DIALS, AIMLESS	XDS, AIMLESS	DIALS, AIMLESS
Resolution (Å)[a]	1.73 (1.76–1.73)	1.66 (1.69–1.66)	1.60 (1.63–1.60)	1.85 (1.89–1.85)	1.40 (1.42–1.40)	2.14 (2.20–2.14)
R_{pim} (%)	2.1 (49.4)	3.3 (30.3)	3.6 (30.9)	5.6 (27.3)	3.8 (40.5)	7.0 (97.6)
$CC_{1/2}$ (%)	99.9 (75.9)	99.9 (84.7)	99.8 (85.4)	99.3 (85.0)	99.7 (80.7)	99.7 (52.2)
$I/\sigma(I)$	18.0 (1.5)	14.5 (2.5)	11.6 (2.5)	7.3 (1.9)	10.9 (2.2)	8.4 (1.2)
Completeness	100.0 (100.0)	99.8 (97.1)	100.0 (100.0)	99.9 (100.0)	99.0 (99.0)	100.0 (100.0)
Redundancy	13.2 (13.4)	6.7 (5.8)	13.10 (10.77)	3.2 (3.3)	3.12 (2.9)	13.3 (13.8)
Observed reflections	521 104 (28830)	598 472 (24663)	1 289 211 (52104)	207 448 (13009)	443 804 (20052)	545 632 (45803)
Unique reflections	39 368 (2151)	88 890 (4211)	98 360 (4837)	64 213 (3986)	141 933 (6998)	40 916 (3299)
Wilson B. factor ($Å^2$)	28.4	12.8	12.1	19.5	17.0	32.5
Refinement statistics						
Resolution	54.24–1.73	29.43–1.66	42.77–1.60	61.84–1.85	48.53–1.40	36.71–2.14
R_{work} (%)	18.3	15.4	15.6	18.2	15.6	17.9
R_{free} (%)	21.3	18.4	17.7	21.5	17.9	22.6
Number of used reflections	37 407	84 312	93 476	61 014	135 015	38 784
Total number of atoms	2894	5770	5790	5720	5762	5701
Number of waters	153	610	555	239	595	266
Average B-factor						
Protein (A, B chains) ($Å^2$)	36.8	19.2/18.3	17.8/17.2	27.5/28.1	18.7/19.7	27.4/28.5
Active-site ligands[b] (of A- and B-chains) ($Å^2$)		27.7 (NAD^+), 18.6 (FE)	23.6 (NAD^+), 19.6 (FE)	30.2 (NADH/ADPR), 28.31 (FE)	18.4 (ADPR), 15.5 (FE)	46.2 (ADPR), 32.3 (FE)
Waters ($Å^2$)	41.2	30.5	28.2	31.2	29.5	41.2
RMS deviation						
Bond lengths (Å)	0.0049	0.0050	0.0077	0.0048	0.0068	0.0057
Bond angles (°)	1.3	1.3	1.4	1.3	1.4	1.4
Ramachandran plot						
Favoured region (%)	97.92	98.03	98.95	98.16	98.17	97.11
Allowed region (%)	1.30	1.31	0.52	1.31	1.31	2.10
Outlier region (%)	0.78	0.66	0.52	0.52	0.52	0.79
PDB entry	7QNI	7QNJ	7R0P	7R5T	7R3D	7QNF

[a]Values given in parentheses are for the highest resolution shell.; [b]ADPR refers to ADP-ribose.

be simplified to more clearly describe the connection between K_2, the dissociation constant of aldehyde from the ternary complexes, k_{-2}/k_2 and K_{MB} (Eqn 3). It is evident that changes in reaction steps not directly describing rates of association and dissociation of the aldehyde may affect the half-saturation value, but only in the direction of lowering K_{MB} as compared to K_2. Thus, increased values

17424658, 2023, 2, Downloaded from https://febs.onlinelibrary.wiley.com/doi/10.1111/febs.16603 by Uppsala University Karin Boye, Wiley Online Library on [17/03/2023]. See the Terms and Conditions (https://onlinelibrary.wiley.com/terms-and-conditions) on Wiley Online Library for rules of use; OA articles are governed by the applicable Creative Commons License

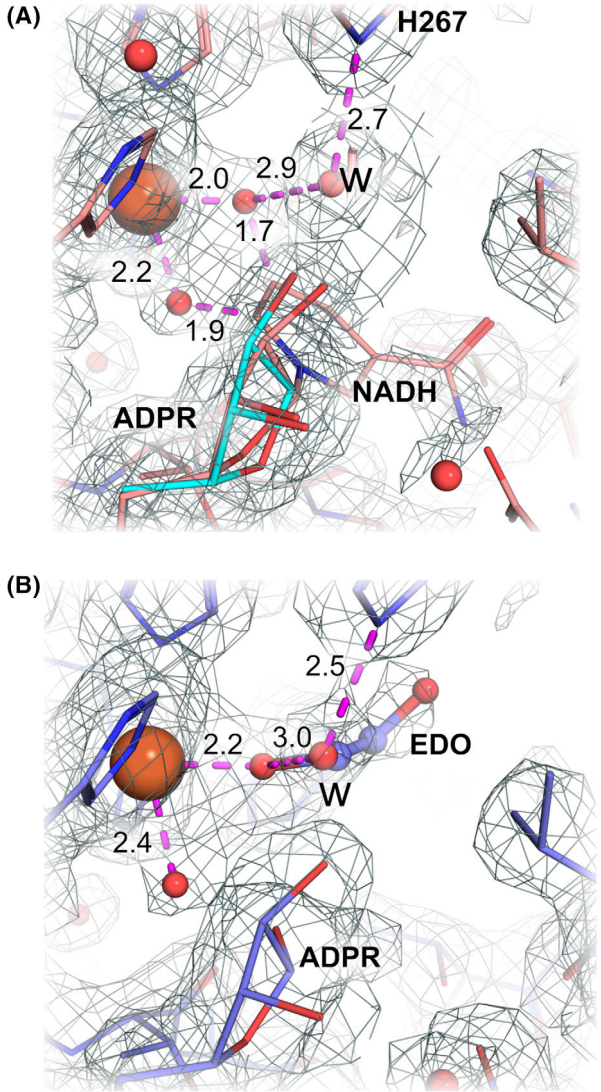

Fig. 6. Alternative conformations of the coenzyme in the active site. (A) In the structure of FucO (F254I) (PDB entry 7R5T, pink coloured carbons), the occupancy of the nicotinamide moiety of the coenzyme is less than unity. The optimal agreement with the modelled electron density is a case where the nicotinamide ring is present but with lower occupancy (0.4) together with an alternative binding mode where the ring is not seen, and the coenzyme is instead modelled as ADP-ribose (ADPR, cyan coloured carbons). Two water molecules coordinated to the iron(II) cofactor cause sterical clashes if the coenzyme is modelled with the ring present. The water molecule labelled "w" is the proposed catalytic proton donor. (B) FucO (N151G/L259V) (B-chain of PDB entry 7QNF, dark blue coloured carbons) cryoprotected with ethylene glycol (EDO). Here, one of the Fe(II)-liganded water molecules is replaced by one of the ligand hydroxyl oxygens, implying a putative substrate-binding mode.

of the half-saturation concentrations suggest mainly effects on association/dissociation of the aldehyde substrates.

$$K_{MB} = \frac{k_5(k_{-2}k_4 + k_{-2}k_{-3} + k_4k_3)}{k_2(k_4k_5 + k_3k_4 + k_3k_5 + k_{-3}k_5)} \quad (2)$$

$$K_{MB} = \frac{K_2}{1 + \frac{k_3k_4}{k_5(k_4+k_{-3})} + \frac{k_3}{k_4+k_{-3}}} \quad (3)$$

Keeping in mind that the displayed cooperativity complicates direct comparisons with ideally behaving model systems (although neither mutant displayed significant cooperativity with **2**), the discussion may still assist in the analysis of the FucO kinetics behaviour.

As judged from the crystal structures, the formation of correct hydrogen bond networks at the active site is expected to facilitate productive aldehyde binding and if disrupted by changes in hydrogen bond donors/acceptors decreased association rate (or increased dissociation rate, or both) could be an effect, resulting in elevated values of K_2. Treating the determined $K_{0.5}$ values as approximations of K_2, the estimated loss in binding energy corresponds to 1.4–2 kcal·mol^{-1}, which is well in agreement with the loss of a hydrogen bond. Such an interpretation implies that the hydrogen bond pattern would change in a manner that interactions between the carbonyl oxygen and the catalytic water molecule are lost. However, in order for such a scenario to be valid, the rate of protonation of the transient alkoxide cannot be affected to a degree where it becomes rate limiting for turnover. An alternative possibility involves also changed interactions with the coenzyme. An effect by the mentioned substitutions was a substantial increase in the respective $K_{0.5}$ values for NADH (Table 1). In an ordered mechanism K_M for NADH, "K_{MA}" is defined by Eq. 4 [13].

$$K_{MA} = \frac{k_3k_4k_5}{k_1(k_4k_5 + k_3k_4 + k_3k_5 + k_{-3}k_5)} \quad (4)$$

which can be reparametrized into,

$$K_{MA} = \frac{K_1}{k_{-1}\left(\frac{1}{k_3} + \frac{1}{k_4} + \frac{1}{k_5} + \frac{K_3}{k_4}\right)} \quad (5)$$

where K_1 is the equilibrium dissociation constant of NADH from the binary E•NADH complex (k_{-1}/k_1) (Table 1) and K_3 is the ratio of reverse and forward fluxes through the redox step. In order for K_{MA} to equal K_1, the sum of all inverse forward-striving terms in the denominator of Eq. 5 should be $1/k_{-1}$. In the wild-type enzyme, the values of K_1 and $K_{0.5}$ for NADH are essentially identical (Table 1). In both mutants, however, $K_{0.5}$ for NADH > K_1. Considering that the mutations in H267Q and D360N supposedly disrupt hydrogen bond networks that

17424658, 2023, 2, Downloaded from https://febs.onlinelibrary.wiley.com/doi/10.1111/febs.16603 by Uppsala University Karin Boye, Wiley Online Library on [17/03/2023]. See the Terms and Conditions (https://onlinelibrary.wiley.com/terms-and-conditions) on Wiley Online Library for rules of use; OA articles are governed by the applicable Creative Commons License

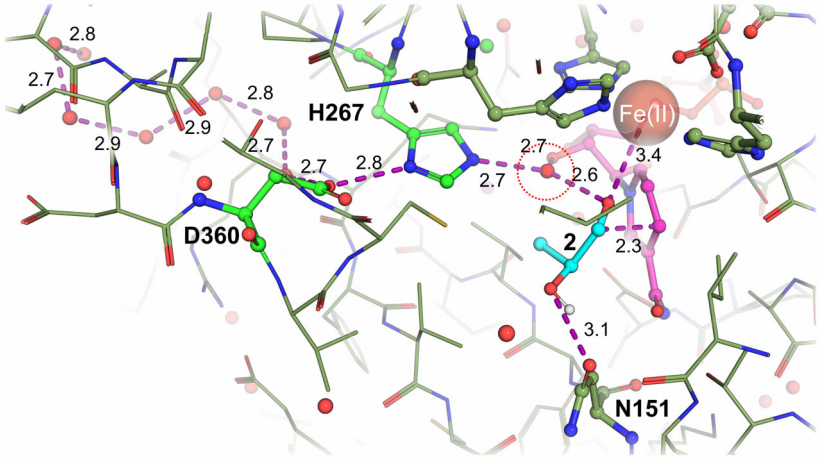

Fig. 7. Hydrogen bond network involving H267 and D360. The NE2 of H267 is via a bridging water molecule (also referred to as the catalytic water, inside dotted ring) connected to the carbonyl oxygen of bound **2** when the substrate is placed in a presumably productive pose. The catalytic water is also hydrogen bonded (at a distance of 2.7 Å) to the 2′-hydroxyl group of the ribose moiety of the coenzyme. A chain of water molecules connecting the aldehyde oxygen to bulk solvent, and including H267 and D360, is evident from the structure. Such a chain of connected waters and acid/base functionalities may act as a provider of protons for the formation of the 1° alcohol product. Image constructed in PyMOL ver. 2.5 using the atomic coordinates in PDB entry 7QNJ.

may influence binding of the second substrate, the reaction step that is most likely to become affected is the dissociation of the alcohol product (with rate constant k_4), since intermolecular interactions with the enzyme are expected to be similar. An increase in the value of k_4 lowers the product value of the denominator resulting in K_{MA} increases as compared to K_1. The proposed catalytic water molecule is also within hydrogen bond distance to the 2′-hydroxyl of the coenzyme ribose (Fig. 7) and it is plausible that this interaction is weakened or lost as a consequence of the D360N/H267Q mutations; a resulting change in the local hydrogen bond network in the presence of substrate, as outlined in Fig. 9, could lower the affinity for NADH and thus result in the observed effects also on the (apparent) $K_{0.5}$ values for the aldehyde substrates. A possibly similar case has been described in the horse liver ADH where picolinimidylation of a coenzyme-interacting Lys residue resulted in similar effects – K_M increases for both coenzymes and second substrates, with retained and even elevated, turnover rates [36].

A possible alternative explanation includes structural dynamics as a component that may influence coenzyme and aldehyde interactions in the active site. If the affinity for the aldehyde substrate is affected by an enzyme form in which the coenzyme is first bound, or *vice versa*, i.e. the enzyme adopts a coenzyme-dependent conformation that provides higher affinity for the second substrate, a lowering of the affinity for NADH would show up as a concomitant (apparent) decrease in affinity for the aldehyde. This would be manifested in steady-state measurements where the coenzyme concentrations are not fully saturating, as in the current study. The described possible model, however, also requires that the affinity of NADH is influenced by binding of the aldehyde, a scenario that is excluded by a linear ordered sequential model. Hence, formation of the ternary E•NADH•R=O complex must be modelled as a random process where the aldehyde may bind to the active site irrespective of preceding NADH binding (Scheme 2). If applying Scheme 2 as a plausible model of substrate binding events, K_M^{NADH} would be dependent on the degree of saturation of the E•R=O binary complex and the ratio of k_{-4}/k_4 which would be distinct from K_1 (k_{-1}/k_1).

Solid evidence for structural dynamics in the group I ADH from horse liver exists [17,37]. The different conformational states (“open” and “closed”) have been linked to distinct kinetic behaviour and binding of the coenzyme stabilizes the closed state, which also exhibits higher affinity for the second substrate [17,36]. Similar coupling between structural states and rate-limiting steps have also been suggested for FucO, but without supporting structural data [23]. We have crystallized a point mutation variant of FucO (L259V) in the absence (“apo”) of coenzyme (NADH or NAD^+) and Fe(II) ion in the active sites and compared its structure with a “holo” enzyme, with bound Fe(II) and coenzyme (Fig. 10). The holo structure is in the closed state, like the wild type, but in the apo structure the domains have adopted a different position with

17424658, 2023, 2, Downloaded from https://febs.onlinelibrary.wiley.com/doi/10.1111/febs.16603 by Uppsala University Karin Boye, Wiley Online Library on [17/03/2023]. See the Terms and Conditions (https://onlinelibrary.wiley.com/terms-and-conditions) on Wiley Online Library for rules of use; OA articles are governed by the applicable Creative Commons License

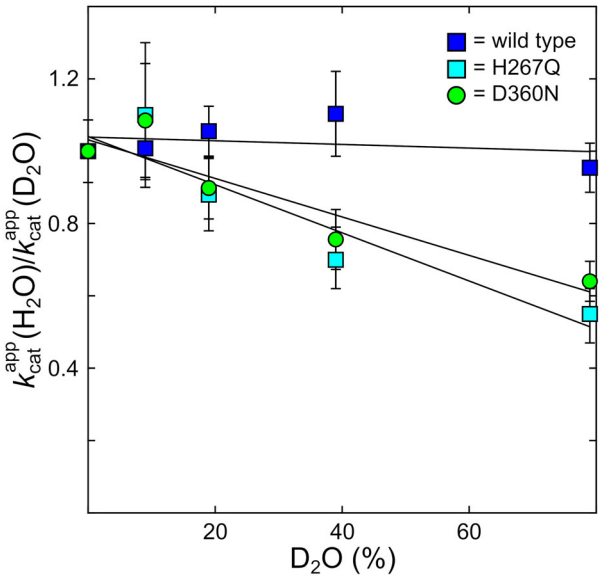

Fig. 8. Proton inventory. The ratios of apparent k_{cat} values of FucO catalysed reduction of **1** determined at different concentrations of D_2O. pL = 8.0, where pL is the negative logarithm of ($[D^+]+[H^+]$). Error bars indicate standard deviations of apparent k_{cat} ratios ($n \geq 3$). The kinetic isotope effects (Table 2) were estimated after fitting a linear model.

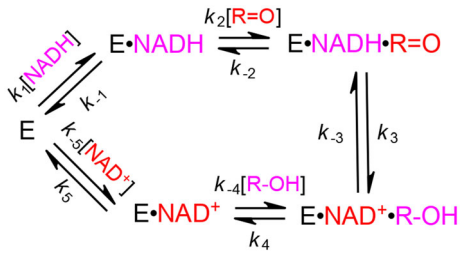

Scheme 1. Ordered sequential BiBi mechanism as working model for FucO catalysed aldehyde reduction.

respect to each other, such that the cleft between the two domains is much wider and we will refer to this state as "open" (Fig. 10). The enlargement of the cleft is the result of rigid-body movements of the nucleotide binding and α-helical domains of approximately 20 degrees with respect to each other, similarly as observed for the equine ADH [37], although the observed differences between the apo and holo states are considerably larger in FucO. In addition, the monomer–monomer interface interactions are different in the apo and holo form (Fig. 10), which correlates with the notion of cooperativity that has been observed in the kinetic studies. Although the apo enzyme form can be viewed as a "non-physiological" state since the protein lacks both the coenzyme, in

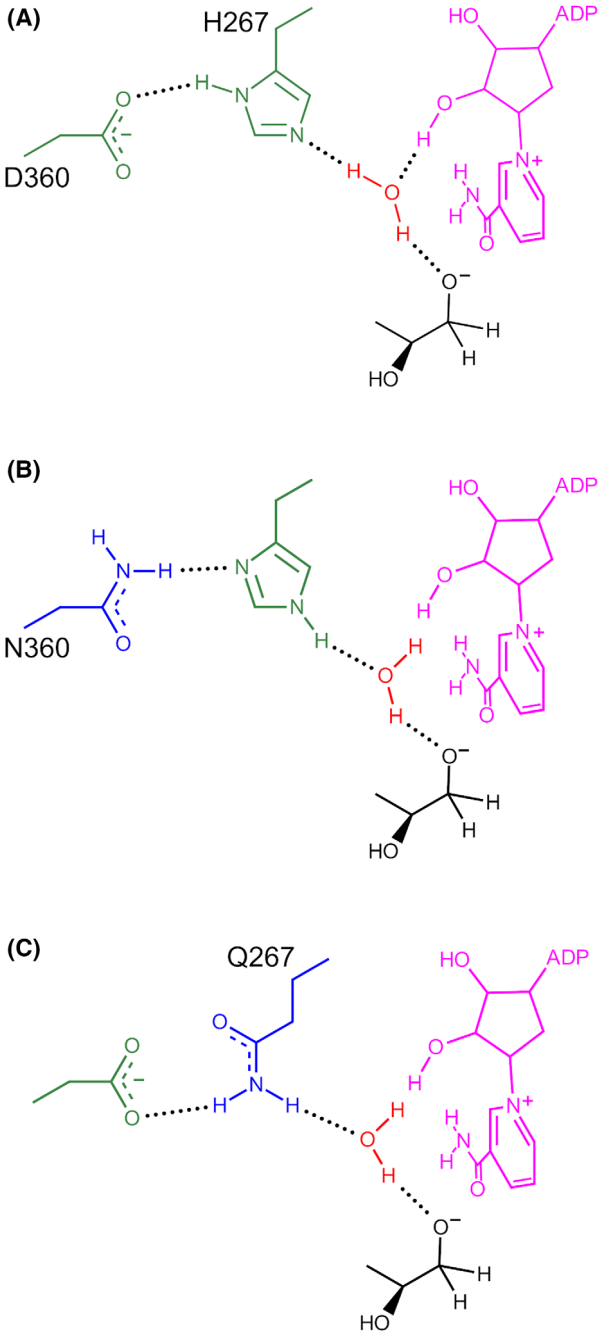

Fig. 9. Possible effects by the H267Q and D360N substitutions on hydrogen bond networks within the active site. (A) In the native enzyme, a hydrogen bond between the proposed catalytic water molecule (red) and the 2′-hydroxyl of the coenzyme ribose can be envisioned, maintaining the capacity for protonation of the transient alkoxide formed in the reduction process. Replacement of either D360 or H267 into Asn (B) and Gln (C), respectively, is expected to change the hydrogen bond interactions of residue H267 into a donor rather than as an acceptor, thereby flipping the orientation of the catalytic water. The end effect would be the loss of a hydrogen bond to the coenzyme.

17424658, 2023, 2, Downloaded from https://febs.onlinelibrary.wiley.com/doi/10.1111/febs.16603 by Uppsala University Karin Boye, Wiley Online Library on [17/03/2023]. See the Terms and Conditions (https://onlinelibrary.wiley.com/terms-and-conditions) on Wiley Online Library for rules of use; OA articles are governed by the applicable Creative Commons License

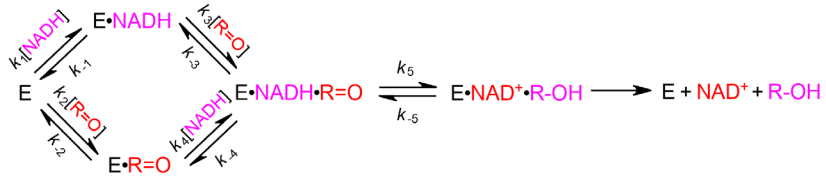

Scheme 2. Random order of binding of NADH coenzyme and aldehyde substrate suggested from the kinetic data in the reduction of **1** catalysed by FucO H267Q and D360N mutants.

either reduced or oxidized form, or the Fe(II) cofactor, the structure demonstrates an intrinsic high degree of conformational flexibility in regions directly responsible for substrate binding and for the organization of a catalytically competent active site.

The solvent deuterium KIE on k_{cat} of the H267Q and D360N mutants in the reaction with **1** is distinct from that of the wild-type displaying *inverse* KIEs (0.38 and 0.50, respectively) (Table 2, Fig. 8). The proton inventories of either mutant are too narrow to allow to conclusively determine the number of hydrogenic sites that cause the observed KIEs. However, the agreement of a linear model of the data suggests that the observed isotope effects may be attributed to single hydrogenic sites. Although the H267Q and D360N substitutions do not affect k_{cat} with either **1** or **2** (Table 1), the displayed inverse solvent deuterium KIEs suggest that *tightening* of hydrogenic sites is at play in the rate-limiting steps of the catalytic cycle [38]. One possible (trivial) explanation is that hydrogen bond networks involved in coenzyme binding are strengthened due to deuteration [39] and thereby restore, in a D_2O-concentration-dependent manner, the affinity for NADH. An increasingly larger proportion of enzymes with productively bound substrates, E•NADH(•R=O), would be reflected as an apparent increase in k_{cat} when reactions are assayed under subsaturating conditions. A direct effect on the chemistry is less likely since proton transfer reactions are not rate limiting, as judged by the absence of a solvent deuterium KIE in the wild-type enzyme. In the case of H267Q, the kinetic isotope effect on k_{cat} in the hydride transfer from NADH to **2** is smaller as compared to that of the wild-type catalysed reaction (2.7 ± 0.4). This suggests that rate limitation has shifted from hydride transfer to include also later steps of the catalytic cycle, i.e. product(s) release.

Conclusions

An ordered BiBi sequential model suffices to describe the kinetics of wild-type FucO, although cooperative behaviour in the kinetics obfuscates the analysis. Reduction chemistry is rate-limiting, as judged by the relatively large primary deuterium kinetic isotope effect on k_{cat}. Protonation of the transient alkoxide is proposed to be delivered by a catalytic water molecule, hydrogen bonded to the coenzyme and a conserved His (H267). Proton supply to the catalytic water molecule is achieved via a hydrogen bond chain connecting bulk solvent with the active site (Fig. 7). The stereoselectivity for (2*S*)-hydroxylated substrates is explained by its direct interaction with the amide side-chain of N151. The enzyme exhibits intrinsic potential for functional structural dynamics as illustrated by large domain movements between an apo form and a cofactor saturated enzyme form and by alternative positions of the coenzyme nicotinamide ring in the determined structures. We propose that domain movement may be important for substrate and coenzyme binding/dissociation kinetics, similarly to the equine liver ADH. Mutations of amino acid residues involved in the chain of hydrogen bonds connecting substrate with the catalytic water molecule and one of the ribose of bound coenzyme apparently shifts the kinetic model to random order of substrate/coenzyme binding, as judged by substantially increased values of half-saturation concentrations but with retained affinity for NADH in the binary E•coenzyme complex.

Materials and methods

Chemicals, reagents and molecular biology components

Buffer components and other bulk chemicals were of the highest purity commercially available. Propanal (**1**, ≥ 97%) (Sigma/Aldrich #W292303, Darmstadt, Germany) and (*S*)-lactaldehyde (**2**, 1 M solution in H_2O) (Sigma/Aldrich #47014), NADH (disodium salt, Sigma/Aldrich #N8129) and NAD^+ (Sigma/Aldrich #443410) were used in reactions as provided by the manufacturer. Oligonucleotides were custom synthesized by Thermo Scientific, Heidelberg, Germany. QuikChange mutagenesis kit and *Escherichia coli* XL-1 Blue were purchased from Agilent, Santa Clara, CA, USA.

17424658, 2023, 2, Downloaded from https://febs.onlinelibrary.wiley.com/doi/10.1111/febs.16603 by Uppsala University Karin Boye, Wiley Online Library on [17/03/2023]. See the Terms and Conditions (https://onlinelibrary.wiley.com/terms-and-conditions) on Wiley Online Library for rules of use; OA articles are governed by the applicable Creative Commons License

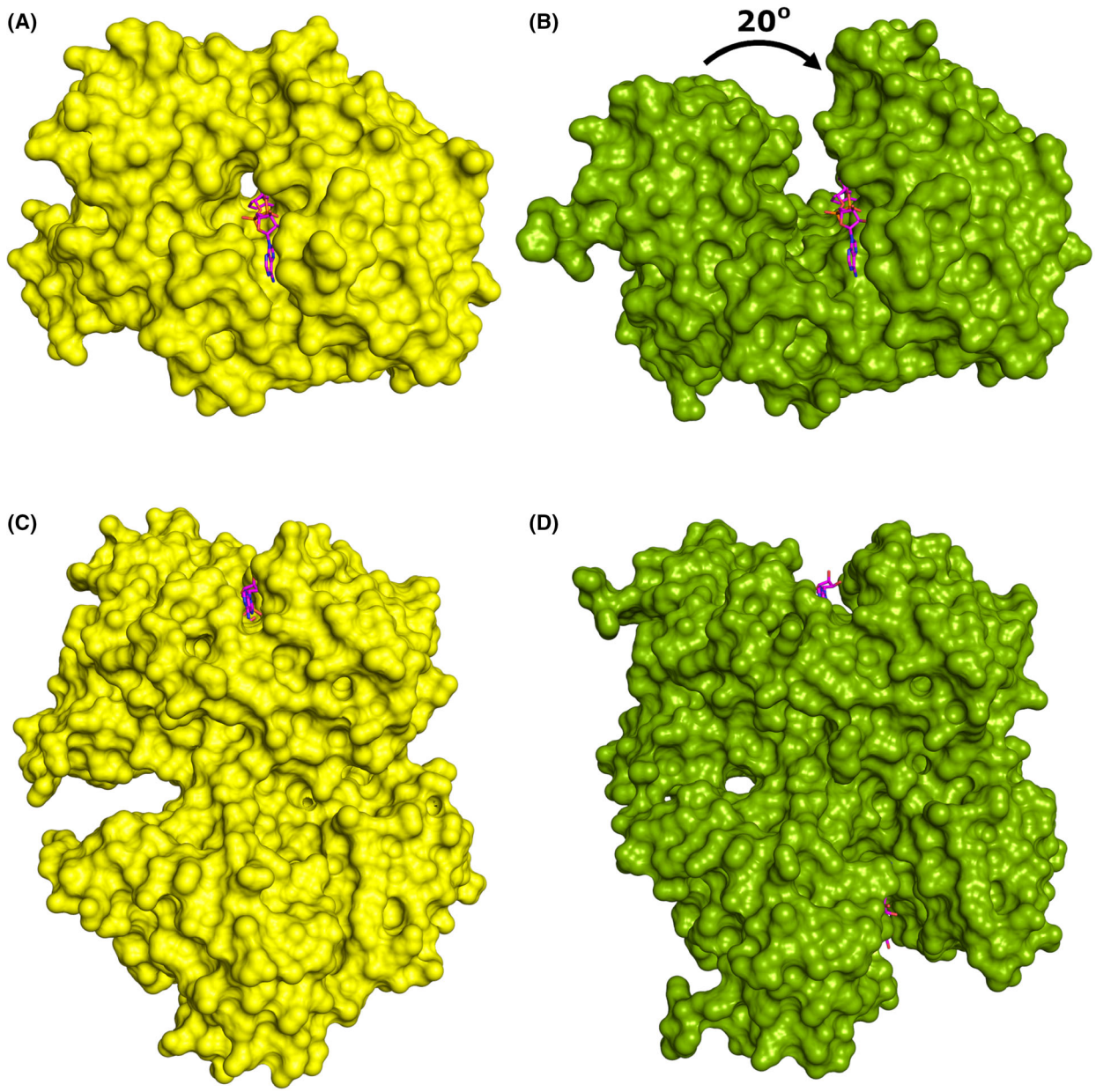

Fig. 10. Crystal structures of a single subunit (A, yellow) and dimer (C, yellow) of the holo form of FucO F254I, with bound NADH and Fe(II) (PDB entry 7R5T) and a single subunit (B, green) and dimer (D, green) of the apo form of FucO L259V, lacking both coenzyme and Fe(II) cofactor (PDB entry 7QNI). The view of the upper subunit of the dimer (shown in C, D) is similar as used for the single subunit (shown in A, B) and the dimer twofold axis runs horizontally between the two subunits of the dimer. The bound NADH molecule in the holo enzyme is shown in stick representation (magenta coloured carbons). The virtual positioning of NADH shown in the apo form panels is obtained by superpositioning of either the C-α-atoms of the residues of the nucleotide binding domain (B) or the dimer (D). The positioning of NADH in the apo structure indicates how domain movements are expected to influence coenzyme interactions with the enzyme. In the apo form, the helical domain has undergone an approximately 20-degree rigid-body rotation with respect to the nucleotide-binding domain, most clearly seen by comparing the A and B panels. The more extended dimer interface of the apo form in comparison with the holo form is seen by comparing the C and D panels.

Site-directed mutagenesis

Mutant genes encoding FucO H267Q and D360N were constructed by the QuikChange (Agilent) protocol by the inclusion of mutameric oligos (Table S2). The desired gene sequences were confirmed by DNA sequencing (Eurofins, Ebersberg, Germany).

17424658, 2023, 2, Downloaded from https://febs.onlinelibrary.wiley.com/doi/10.1111/febs.16603 by Uppsala University Karin Boye, Wiley Online Library on [17/03/2023]. See the Terms and Conditions (https://onlinelibrary.wiley.com/terms-and-conditions) on Wiley Online Library for rules of use; OA articles are governed by the applicable Creative Commons License

Protein expression and purification

The wild-type enzyme and variants thereof were expressed and purified as described previously [23].

Sequence alignment, protein crystallization, data collection, processing and structure determination

CLUSTALW analysis [40] was performed for a selection of protein Blast [41] hits. The chosen protein sequences were within a score range of 317–200 bits applying the default settings in the BLASTP program as provided by the Expasy service (Swiss Institute of Bioinformatics, Lausanne, Switzerland, www.expasy.org).

Protein crystals of the different FucO variants were obtained in the conditions specified in Table S3. The crystal treatment is also specified in Table S3 and the data sets were collected from cryocooled crystals (Table 3). The data sets were processed using XDS (7QNI, 7QNJ and 7R3D) [42,43] or DIALS (7QNF, 7R0P and 7R5T) [44], as specified also in Table 3. Data were further scaled and merged using AIMLESS [45]. The crystal structures were solved by the molecular replacement method using molecule A of PDB entry 1RRM [30] as the search model. The molecule was split into two parts consisting of domain A (residues 1–185) and domain B (residues 186–383), and the structure was determined using the expert mode of the molecular replacement program PHASER [46] from ccp4i2 [47]. One (FucO L259V, apo, PDB entry 7QNI) or two copies (all other structures) of each protein subunit were obtained as solutions of the molecular replacement calculations, and the correct orientation of the domains in the molecules was selected using the symmetry operations in COOT [48]. COOT was used to manually improve the protein model and identify the ligands and the waters. The structure was further refined using REFMAC5 [49]. Refinement statistics are given in Table 3. The quality of the structure was checked by using the validation tools of COOT and by inspecting the PDB validation report. In the refined structures of the complexes with NAD^+ or NADH, it was noticed that the electron density map around the nicotinamide ring was usually weaker than for the rest of the nucleotide, suggesting either (a) the nicotinamide ring is disordered or (b) NAD^+/NADH was partially hydrolysed, forming adenosine diphosphate ribose (ADPR). In the structure where the density for the nicotinamide ring was poor, the nucleotide was modelled as ADPR (PDB entries 7R3D and 7QNF). In other structures, NAD^+ was included in the model, in which case the B-factors of the nicotinamide moiety were higher than the remaining part (PDB entries 7QNJ, 7R0P). In one structure, the best description was provided by including in the model both ADPR and NADH, with similar occupancy (PDB entry 7R5T).

Molecular modelling

Aldehyde substrate **2** was manually positioned, using PyMOL, in the active site of FucO (F254I). The modelling was guided by the structure of FucO (N151G/L259V, PDB entry 7QNF) cryoprotected with ethylene glycol which is a *bona fide* alcohol substrate. In this structure, the bound nucleotide is modelled as ADPR. The mode of binding of ethylene glycol is shown in Fig. 6B.

Steady-state kinetics

Aldehyde reduction was assayed spectrophotometrically in 0.1 M sodium phosphate, pH 8.0, at 30 °C, by the time-dependent concomitant oxidation of NADH, followed at 340 nm in a 0.5-cm cuvette. NADH concentration was kept at 0.4 mM, which corresponds to $11 \times K_{0.5}$ for the wild-type, $\leq 1.9 \times K_{0.5}$ for the H267Q and D360N mutants. Kinetic parameters were also determined in the presence of varying concentrations of NADH (20–500 μM) and 30 mM **1** or 0.2–20 mM **2**. Stated aldehyde concentrations refer to the sum of the hydrate and aldehydic forms.

Steady-state kinetic parameters were determined after fitting either the Michaelis–Menten equation or a modified Hill equation (Eqn 1), to the experimental data using programs MMFIT or INRATE, respectively, in the Simfit package (www.simfit.org.uk). $K_{0.5}$ in Eqn (1) refers to the half-saturation concentration of the enzyme catalysed reaction and n_H is the Hill coefficient. Model discriminations between the two rate laws were determined by F-tests of the residuals with a threshold of $P < 0.05$ for inclusion of the Hill coefficient in the rate expression.

Product inhibition

The reduction of **2** was followed during the steady state in 0.1 M sodium phosphate pH 8.0, at 30 °C, by recording the initial velocities of NADH reduction at either constant concentrations of **2** (4 mM, $12 \times K_{0.5}$) and varied [NADH] (5–80 μM) or at constant [NADH] (0.4 mM, $10 \times K_M$) and varied [**2**] (0.4–20 mM) in the presence of different concentrations of product, either NAD^+ (0–270 μM) or **4** (0–450 mM). Kinetic parameters were determined as described above and the inhibition patterns were analysed by double reciprocal plots of initial reaction velocities as functions of varied [**2**] or [NADH], respectively, in the presence of the different concentrations of either NAD^+ or **4** as inhibitors.

Proton inventory

Catalysed rates were determined in the presence of 0.4 mM NADH and 5 mM **1** and 20 nM of wild-type or 60 mM **1** and 20 nM of H267Q and D360N. Reactions were performed in D_2O/H_2O ratios between 0 and 79%, in 0.1 M

17424658, 2023, 2, Downloaded from https://febs.onlinelibrary.wiley.com/doi/10.1111/febs.16603 by Uppsala University Karin Boye, Wiley Online Library on [17/03/2023]. See the Terms and Conditions (https://onlinelibrary.wiley.com/terms-and-conditions) on Wiley Online Library for rules of use; OA articles are governed by the applicable Creative Commons License

sodium-phosphate, at 30 °C (pL = 8). pL was adjusted using a pH meter applying the following compensation: pL = pD + 0.3139α + 0.085α^2 [50], where pD is the value of the glass electrode reading and α is the fraction of D_2O/H_2O.

Kinetic isotope effect in hydride transfer from NADH to aldehyde

[4*R*-^{2}H]NADH (A-side NADD (nicotinamide adenine dinucleotide)) was synthesized as described in [23] which is a revised protocol of Hallis and Liu [51]. As many as 860 units of yeast alcohol dehydrogenase, 0.14 mmol NAD^+ and 8.5 mmol ethanol-d_5 (Sigma Aldrich #489336) added in portions of 1.7 mmol every 20 min were mixed in 15 mL 50 mM NH_4HCO_3 and incubated at room temperature for 1.5 h. Kinetic isotope effects (KIEs) in aldehyde reduction were determined in the presence of 0.4 mM [4*R*-^{2}H]NADH/NADH (50 : 50) and varying concentrations (0.125–5 mM) of **2** for wild-type and (5–30 mM) for H267Q.

Pre-steady-state kinetics

The association and dissociation rates of enzyme/NADH were determined in stopped-flow experiments in an Applied Photophysics SX-20 fluorometer. NADH fluorescence was excited at 340 nm and emitted light was collected above 405 nm. Slit widths for entering and exiting light were set to 1 mm. Enzyme (5 μM) was rapidly mixed with NADH (20–60 μM) and the transient exponential increase in fluorescence emission was recorded. The apparent rates, k_{obs}, reflecting the approach to the association/dissociation equilibrium were determined by fitting Eqn (6) to the experimental trace averages, where F is the recorded emitted light, A, the signal amplitude and C the floating end point. The rate constants of NADH association, k_{on}, and dissociation, k_{off}, were determined after fitting Eqn (7) to the determined values of k_{obs}. Examples of averaged fluorescence tracks and fits of Eqns (6) and (7) are shown in Fig. S2.

$$F = A\exp(-k_{obs}t) + C \quad (6)$$

$$k_{obs} = k_{on}[NADH] + k_{off} \quad (7)$$

Acknowledgements

The synchrotron data sets were collected at beamline P14 operated by EMBL Hamburg at the PETRA III storage ring (DESY, Hamburg, Germany) and beamlines I03 and I24 at Diamond Light Source (Oxford, UK). We thank the beamline scientists for their expert assistance when using these beamlines. The use of the facilities and expertise of the Biocenter Oulu Structural Biology Core Facility, a member of Biocenter Finland, Instruct-ERIC Centre Finland and FINStruct, are gratefully acknowledged. We thank Dr Subhadra Dalwani for preparing Fig. 10. This work was kindly supported by Foundation Olle Engkvist Byggmästare (MW, #194-0638).

Conflict of interest

The authors declare no conflict of interest.

Author contributions

AZ, SS, TRK and RKW conducted the experimental part. All authors participated in data analysis. RKW and MW planned and lead the work. All authors participated in the writing of the manuscript.

Data availability statement

The structures have been deposited in the open access PDB data base, with entry numbers 7QNI, 7QNJ, 7R0P 7R5T, 7R3D and 7QNF.

References

1 Bahnson BJ, Park D-H, Kim K, Plapp BV, Klinman JP. Unmasking of hydrogen tunneling in the horse liver alcohol dehydrogenase reaction by site-directed mutagenesis. *Biochemistry*. 1993;**32**:5503–7.
2 Johnson BJ, Klinman JP. Hydrogen tunneling in enzyme catalysis. *Methods Enzymol*. 1995;**249**:373–97.
3 Layfield JO, Hammes-Schiffer S. Hydrogen tunneling in enzymes and biomimetic models. *Chem Rev*. 2014;**114**:3466–94.
4 Roston D, Islam Z, Kohen A. Kinetic isotope effects as a probe of hydrogen transfers to and from common enzymatic cofactors. *Arch Biochem Biophys*. 2014;**544**:96–104.
5 Cleland WW. Low-barrier hydrogen bonds and enzymatic catalysis. *Arch Biochem Biophys*. 2000;**382**:1–5.
6 Auld DS, Bergman T. The role of zinc for alcohol dehydrogenase structure and function. *Cell Mol Life Sci*. 2008;**65**:3961–70.
7 Scharschmidt M, Fisher MA, Cleland WW. Variation of transition-state structure as a function of the nucleotide in reactions catalyzed by dehydrogenases. 1. Liver alcohol dehydrogenase with benzyl alcohol and yeast aldehyde dehydrogenase with benzaldehyde. *Biochemistry*. 1984;**23**:5471–8.

17424658, 2023, 2, Downloaded from https://febs.onlinelibrary.wiley.com/doi/10.1111/febs.16603 by Uppsala University Karin Boye, Wiley Online Library on [17/03/2023]. See the Terms and Conditions (https://onlinelibrary.wiley.com/terms-and-conditions) on Wiley Online Library for rules of use; OA articles are governed by the applicable Creative Commons License

8 Hammes-Schiffer S. Comparison of hydride, hydrogen atom, and proton-coupled electron transfer reactions. *ChemPhysChem*. 2002;**3**:33–42.
9 Theorell H, Bonnichsen R. Studies on liver alcohol dehydrogenase. I. Equilibria and initial rate velocities. *Acta Chem Scand*. 1951;**5**:1105–26.
10 Theorell H, Chance B. Studies on liver alcohol dehydrogenase. II. The kinetics of the compound of horse liver alcohol dehydrogenase and reduced diphosphopyridine nucleotide. *Acta Chem Scand*. 1951;**5**:1127–44.
11 Wratten CC, Cleland WW. Kinetic studies with liver alcohol dehydrogenase. *Biochemistry*. 1965;**11**:2442–51.
12 Shore JD, Gutfreund H. Transients in the reactions of liver alcohol dehydrogenase. *Biochemistry*. 1970;**9**:4655–9.
13 Plapp BV. On calculation of rate and dissociation constants from kinetic constants for the ordered bi bi mechanism of liver alcohol dehydrogenase. *Arch Biochem Biophys*. 1973;**156**:112–4.
14 Ganzhorn AJ, Green DW, Hershey AD, Gould RM, Plapp BV. Kinetic characterization of yeast alcohol dehydrogenases. Amino acid residue 294 and substrate specificity. *J Biol Chem*. 1987;**262**:3754–61.
15 Sekhar VC, Plapp BV. Rate constants for a mechanism including intermediates in the interconversion of ternary complexes by horse liver alcohol dehydrogenase. *Biochemistry*. 1990;**29**:4289–95.
16 Hamnevik E, Blikstad C, Norrehed S, Widersten M. Kinetic characterization of *Rhodococcus ruber* DSM 44541 alcohol dehydrogenase a. *J Mol Catal B Enzymol*. 2014;**99**:68–78.
17 Plapp BV. Conformational changes and catalysis by alcohol dehydrogenase. *Arch Biochem Biophys*. 2010;**493**:3–12.
18 Baskar Raj S, Ramaswamy S, Plapp BV. Yeast alcohol dehydrogenase structure and catalysis. *Biochemistry*. 2014;**53**:5791–803.
19 The PyMOL Molecular Graphics System, Version 2.0. Schrödinger, LLC.
20 Reid MF, Fewson CA. Molecular characterization of microbial alcohol dehydrogenases. *Crit Rev Microbiol*. 1994;**20**:13–56.
21 Baldomá L, Aguilar J. Metabolism of L-fucose and L-rhamnose in *Escherichia coli*: aerobic-anaerobic regulation of L-lactaldehyde dissimilation. *J Bacteriol*. 1988;**170**:416–21.
22 Conway T, Ingram LO. Similarity of *Escherichia coli* propanediol oxidoreductase (*fucO* product) and an unusual alcohol dehydrogenase from *Zymomonas mobilis* and *Saccharomyces cerevisiae*. *J Bacteriol*. 1989;**171**:3754–9.
23 Blikstad C, Widersten M. Functional characterization of a stereospecific diol dehydrogenase, FucO, from *Escherichia coli*: substrate specificity, pH dependence, kinetic isotope effects and influence of solvent viscosity. *J Mol Catal B Enzymol*. 2010;**66**:148–55.
24 Blikstad C, Dahlström KM, Salminen TA, Widersten M. Stereoselective oxidation of aryl-substituted vicinal diols into chiral α-hydroxy aldehydes by re-engineered propanediol oxidoreductase. *ACS Catal*. 2013;**3**:3016–25.
25 Blikstad C, Dahlström KM, Salminen TA, Widersten M. Substrate scope and selectivity in offspring to an enzyme subjected to directed evolution. *FEBS J*. 2014;**281**:2387–98.
26 Gutfreund H. Behavior and analysis of rapid equilibrium and steady-state enzyme systems. In: Segel IH, editor. Enzyme kinetics. New York, NY: John Wiley & Sons, Inc.; 1975. p. 649–56.
27 Friedrich P. On the physiological significance of positive and negative cooperativity in enzymes. *J Theor Biol*. 1979;**81**:527–32.
28 Goldbeter A, Venieratos D. Analysis of the role of enzyme co-operativity in metabolic oscillations. *J Mol Biol*. 1980;**138**:137–44.
29 Northrop DB. The expression of isotope effects on enzyme.Catalyzed reactions. *Annu Rev Biochem*. 1981;**50**:103–31.
30 Kumaran D, Swaminathan S. Crystal structure of Lactaldehyde reductase. 2004. https://doi.org/10.2210/pdb1rrm/pdb
31 Moon J-H, Lee H-J, Park S-Y, Song J-M, Park M-Y, Park H-M, et al. Structures of iron-dependent alcohol dehydrogenase 2 from *Zymomonas mobilis* ZM4 with and without NAD^+ cofactor. *J Mol Biol*. 2011;**407**:413–24.
32 Marcal D, Rêgo AT, Carrondo MA, Enguita FJ. 1,3-propanediol dehydrogenase from *Klebsiella pneumoniae*: decameric quaternary structure and possible subunit cooperativity. *J Bacteriol*. 2009;**191**:1143–51.
33 Larson SB, Jones JA, McPherson A. The structure of an iron-containing alcohol dehydrogenase from a hyperthermophilic archaeon in two chemical states. *Acta Crystallogr*. 2019;**F75**:217–26.
34 Schwarzenbacher R, von Delft F, Canaves JM, Brinen LS, Dai X, Deacon AM, et al. Crystal structure of an iron-containing 1,3-propanediol dehydrogenase (TM0920) from *Thermotoga maritima* at 1.3 Å resolution. *Proteins*. 2004;**54**:174–7.
35 Azmi L, Bragginton EC, Cadby IT, Byron O, Roe AJ, Lovering AL, et al. High-resolution structure of the alcohol dehydrogenase domain of the bifunctional bacterial enzyme AdhE. *Acta Crystallogr*. 2020; **F76**:414–21.
36 Plapp BV, Brooks RL, Shore JD. Horse liver alcohol dehydrogenase. Amino groups and rate-limiting steps in catalysis. *J Biol Chem*. 1973;**248**:3470–5.
37 Eklund H, Samama J-P, Wallén L, Bränden C-I, Åkeson Å, Jones TA. Structure of a triclinic ternary complex of horse liver alcohol dehydrogenase at 2.9 Å resolution. *J Mol Biol*. 1981;**146**:561–87.

17424658, 2023, 2, Downloaded from https://febs.onlinelibrary.wiley.com/doi/10.1111/febs.16603 by Uppsala University Karin Boye, Wiley Online Library on [17/03/2023]. See the Terms and Conditions (https://onlinelibrary.wiley.com/terms-and-conditions) on Wiley Online Library for rules of use; OA articles are governed by the applicable Creative Commons License

38 Schowen KB, Schowen RL. Solvent isotope effects on enzyme systems. *Methods Enzymol*. 1982;**87**:551–606.
39 Scheiner S, Čuma M. Relative stability of hydrogen and deuterium bonds. *J Am Chem Soc*. 1996;**118**:1511–21.
40 Larkin MA, Blackshields G, Brown NP, Chenna R, McGettigan PA, McWilliam H, et al. Clustal W and Clustal X version 2.0. *Bioinformatics*. 2007;**23**:2947–8.
41 Altschul SF, Gish W, Miller W, Myers EW, Lipman DJ. Basic local alignment search tool. *J Mol Biol*. 1990;**215**:403–10.
42 Kabsch W. XDS. *Acta Crystallogr D Biol Crystallogr*. 2010;**66**:125–32.
43 Sparta KM, Krug M, Heinemann U, Mueller U, Weiss MS. XDSAPP2.0. *J Appl Cryst*. 2016;**49**:1085–92.
44 Winter G, Waterman DG, Parkhurst JM, Brewster AS, Gildea RJ, Gerstel M, et al. DIALS: implementation and evaluation of a new integration package. *Acta Crystallogr D Struct Biol*. 2018;**74**:85–97.
45 Evans PR, Murshudov GN. How good are my data and what is the resolution? *Acta Crystallogr D Biol Crystallogr*. 2013;**69**:1204–14.
46 McCoy AJ, Grosse-Kunstleve RW, Adams PD, Winn MD, Storoni LC, Read RJ. Phaser crystallographic software. *J Appl Crystallogr*. 2007;**40**:658–74.
47 Potterton L, Agirre J, Ballard C, Cowtan K, Dodson E, Evans PR, et al. CCP4i2: the new graphical user interface to the CCP4 program suite. *Acta Crystallogr D Struct Biol*. 2018;**74**:68–84.
48 Casañal A, Lohkamp B, Emsley P. Current developments in coot for macromolecular model building of electron cryo-microscopy and crystallographic data. *Protein Sci*. 2020;**29**:1069–78.
49 Kovalevskiy O, Nicholls RA, Long F, Carlon A, Murshudov GN. Overview of refinement procedures within REFMAC5: utilizing data from different sources. *Acta Crystallogr D Struct Biol*. 2018;**74**:215–27.
50 Pentz L, Thornton ER. Isotope effects on the basicity of 2-nitrophenoxide, 2,4-dinitrophenoxide, hydroxide, and imidazole in protium oxide-deuterium oxide mixtures. *J Am Chem Soc*. 1967;**89**:6931–8.
51 Hallis TM, Liu H. Stereospecificity of hydride transfer for the catalytically recycled NAD^+ in CDP-D-glucose 4,6-dehydratase. *Tetrahedron*. 1998;**54**:15975–82.

Supporting information

Additional supporting information may be found online in the Supporting Information section at the end of the article.

Fig. S1. Sequence alignment (ClustalW) of a selection of FucO relatives.
Fig. S2. Experimental track and model fitting of NADH association/dissociation kinetics.
Table S1. Product inhibition – kinetic parameters.
Table S2. Sequences of deoxyoligonucleotides used in mutagenesis.
Table S3. Crystallization and crystal treatment protocols.

17424658, 2023, 2, Downloaded from https://febs.onlinelibrary.wiley.com/doi/10.1111/febs.16603 by Uppsala University Karin Boye, Wiley Online Library on [17/03/2023]. See the Terms and Conditions (https://onlinelibrary.wiley.com/terms-and-conditions) on Wiley Online Library for rules of use; OA articles are governed by the applicable Creative Commons License